TruffleBot: Low-Cost Multi-Parametric Machine Olfaction

Jason Webster, Pratistha Shakya, Eamonn Kennedy, Michael Caplan, Christopher Rose, and Jacob K. Rosenstein

School of Engineering

Brown University, Providence, RI 02912, USA

Abstract— **This paper presents a low-cost and flexible platform for bio-inspired machine olfaction, which aims to extend traditional electronic nose approaches by adding fluid-mechanical and spatiotemporal dimensions. The *TruffleBot* contains an array of chemical, pressure, and temperature sensors in a small embedded platform. By "sniffing" vapors in a temporally-modulated sequence through four different air paths across eight sensor locations, we introduce spatial and temporal information that significantly enhances classification of odors. Using only chemical time series, we demonstrate 91% cross-validated classification accuracy for nine odors. With the addition of pressure and temperature time series, TruffleBot's classification accuracy can reach 95-98%.**

Keywords— *electronic nose, machine olfaction, odor classification, sensor network, gas sensor, MOX, pressure sensor*

I. INTRODUCTION

A sense of smell is one of the most fundamental ways that animals interact with the world [1]. Many groups have worked towards bio-inspired machine olfaction [2], particularly through the statistical interpretation of a diversity of chemical measurements [3]. However, an important insight into the biological process is that the brain takes advantage of many types of *non*-chemical information when analyzing odors, including temporal, spatial, mechanical, hedonic, and contextual correlations [4], [5]. For example, crayfish antennae contain multiple types of setae whose outputs are processed jointly [6], and mammalian olfactory neurons respond to both odors and pressure changes [7]. In contrast, engineered chemical sensors often ignore this ancillary information [8]–[11], and environmental conditions are often considered only in the context of calibrating chemical measurements [12].

Most implementations of e-noses comprise an array of chemical sensors whose outputs are analyzed in parallel at one discrete point in time. These designs are widely employed across military, industrial, medical, and environmental sciences, with applications ranging from explosives and disease detection to environmental and industrial monitoring [3], [8]–[10], [12]–[15]. Recent advances in compact, portable, and low-cost sensor designs have been complemented by aggressive microelectronic integration [11], [16]–[18].

In this paper, we introduce the TruffleBot, an electronic platform which classifies odors using multi-parametric environmental information in order to improve upon traditional e-noses. The TruffleBot simultaneously samples pressure, temperature, and chemical time series, while "sniffing" in a temporally modulated sequence which introduces spatiotemporal time signatures, such as transport delays and diffusive dynamics. We show how these multidimensional signals depend on chemical and physical properties which can be unique to a particular chemical. Additionally, the odor plumes traverse a set of four different pathways which have the aggregate effect of expanding the feature space and separability of odors. We demonstrate how this approach, which mirrors some of the dynamic contextual features of animal olfaction [5], improves the performance and accuracy of chemical sensing in a simple and low-cost hardware platform.

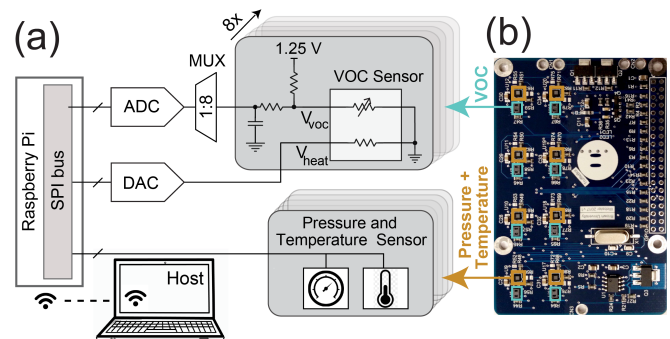## II. SYSTEM ARCHITECTURE AND DESIGN

Fig. 1.   (a) Schematic of the sensing circuits. Eight analog metal-oxide gas sensors are digitized while a DAC controls their heater voltage. Eight digital barometers on the board measure pressure and temperature. (b) An image of the TruffleBot (top view). Pairs of barometers (brown) and chemical sensors (cyan) are arranged in a 4×2 array.

The TruffleBot is designed to be versatile and straightforward to reproduce and modify, and it is implemented as a HAT (Hardware Attached on Top) with the same footprint as a Raspberry Pi (85 mm $\times$ 56 mm). Figure 1 depicts the salient components of the board along with key elements in the electronic signal path. An array of eight sensor pairs are arranged in four rows of two, with each position containing one Volatile Organic Compound (VOC) sensor and one digital barometer.

The VOC sensors (AMS CCS801) are micro-hotplate metal-oxide (MOX) sensors with integrated resistive heaters.

In a MOX gas sensor, a metal oxide film is heated to several hundred degrees Celsius, to a temperature where its electrical conductivity becomes sensitive to chemical interactions with nearby gases. These interactions are complex and non-specific, and MOX sensors will respond to the presence of many different volatile molecules. The heaters of the eight MOX sensors are driven from a common buffered DAC, whose voltage controls the temperature of the sensors, and in turn, affects their chemical sensitivity. The MOX resistivity is converted to a voltage and routed through a multiplexer into a high precision ADC (TI ADS1256).

The digital barometers (ST LPS22HB) are small MEMS sensors with piezoresistive elements on a thin suspended membrane. These chips measure both temperature and absolute pressure at up to 75 samples per second through a serial peripheral interface (SPI) bus.

The TruffleBot is powered entirely through the 5V and 3.3V rails of the Raspberry Pi, and consumes approximately 77 mW. The board also hosts several other supporting circuits, including a precision reference generator for the MOX sensors, and transistors to switch external 5V peripherals which may include solenoids and small air pumps. Other peripherals can also be connected through USB. Including the Raspberry Pi, components for one TruffleBot cost approximately $150.

The TruffleBot connects to a host computer over ethernet or WiFi, and multiple TruffleBots can co-exist on the same network. A Python host program initiates an experiment by broadcasting a command for all TruffleBots to begin data collection. When the trial concludes, the host automatically retrieves the sensor traces from all clients for analysis in MATLAB.

III. Experimental Results

A. Sensor transient response

It is instructive to first consider the response of sensors at a single location in the array. Figure 2 plots the temperature, pressure and chemical response to a five second exposure to odors from beer ($\approx$ 6% ethanol). The output of the VOC sensor is expressed as a percentage of its full scale range, and the pressure and temperature signals deviate only slightly from ambient. When beer odors are introduced, the pressure decreases and the temperature increases; both the polarity and magnitude of these changes depend on the physical properties of the analyte vapor including its vapor pressure, density, and molecular weight. These differences contribute to TruffleBot's overall chemical selectivity, and will be explored in more detail in the following sections.

B. Response to different chemicals

Experiments were performed in the test bench shown in Fig. 3. The output of a pump is regulated to a constant flow, and a three-way solenoid valve (Takasago CTV-3) selectively bypasses the analyte vapor. The solenoid position follows a short binary control sequence, producing a concentration-modulated release of analyte vapor [19], [20]. The analytes used in these experiments were ambient air (control), apple
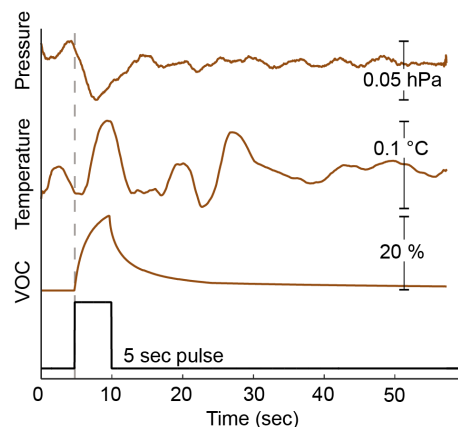

Fig. 2. Example sensor traces from a single array location, in response to odors from beer (Lagunitas IPA, 6.2% ABV). When a constant flow of air (850 sccm) is switched to beer odors for 5 seconds, the VOC sensor resistance decreases, and when it switches back to air, it returns to its initial value. The change in gas composition also produces small correlated changes in the temperature and air pressure.

cider vinegar, lime juice, beer (6.2% ABV), wine (chardonnay, 13% ABV), vodka (40% ABV), ethanol (100% ABV), isopropanol, and acetone. A manifold splits the fluid flow between four small plastic columns that rest on the sensor board. Each column contains different obstructions that affect the airflows reaching the sensor array. (Other researchers have similarly utilized differentially obstructed columns in electronic noses [21], [22].) This arrangement allows us to adjust multiple parameters including the overall airflow, the solenoid's temporal sequence, the analyte, and the geometries and contents of the columns.
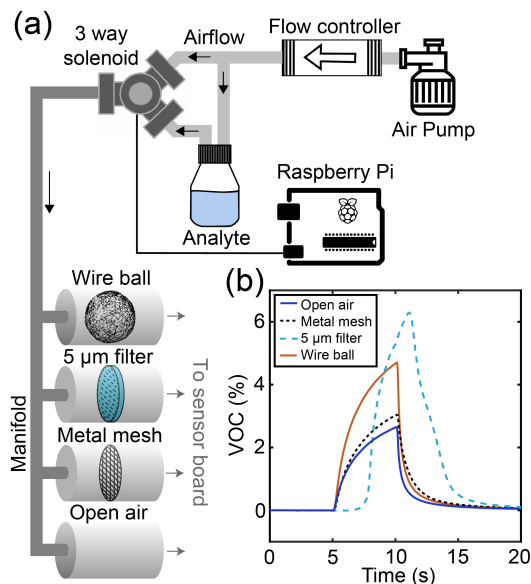

Fig. 3. (a) An illustration of the experimental setup for introducing chemical vapors. A solenoid switches between clean air and analyte vapor, at a constant flow rate. The airflow is then divided between four obstructed paths, which lead to two sensors each. (b) Differences in the positions and obstructions of four air paths produce different signals in each column, in response to ethanol.

Figure 4 shows a comparison of the responses to air, vodka and acetone, at a single array position. The baseline signal levels are affected by noise and uncontrolled parameters including ambient temperature, humidity, and atmospheric

pressure. The solenoid control sequence is the same for all trials, and the signal is represented by temporally correlated changes in the sensor outputs. Assuming a lossless system with fixed volumetric flow, the total absolute pressure in each column head can be represented as

$$P_{abs} = P_{atm} + P_{ext} + P_{analyte} \qquad (1)$$

where P_{ext} is the resulting pressure from the constant regulated airflow and P_{atm} and $P_{analyte}$ are the partial pressures exerted by atmospheric air and analyte vapor. (When the solenoid bypasses the analyte, $P_{analyte} = 0$.) According to the Darcy-Weisbach equation, pressure drop in a Newtonian fluid flowing through a cylindrical tube is given by

$$\Delta p = \frac{\rho f L v^2}{2D} \qquad (2)$$

where ρ is the fluid density, v is the fluid velocity and f, L, D are the friction coefficient, length, and diameter of the tube. Since the flow is constant and tube properties do not change, Δp only depends on ρ. Thus an analyte with vapor density greater than air would incur more pressure loss in the tube, resulting in a decrease in measured air pressure. For example, P_{abs} decreases during the release of beer ($\rho = 1.05$ g/cm^3) but increases for vodka ($\rho = 0.95$ g/cm^3).

These pressure changes, in combination with the analyte's physical properties (*e.g.* heat capacity), produce analyte-specific temperature fluctuations. TruffleBot uses this information to distinguish between analytes which have similar MOX sensor responsivity, provided the pressure and temperature changes observed are a systematic result of the analyte's physical properties. For example, in Fig. 4, vodka and acetone could have been easily discriminated by temperature and pressure alone.

C. Analyte Classification

The arrayed sensors and diverse airflow paths support the extraction of temporal and spatial features. Using the setup in Fig. 3, the same 40-bit "sniffing" sequence was applied at 1 bit/second for 8 different analytes. Representative data for each odor is shown in Fig 5a. The first eight rows represent VOC sensor traces, followed by eight rows of pressure readings and eight rows of temperature readings. The mean value has been subtracted from each trace. The control trials with ambient air show only small deviations, and VOC magnitudes appear to correlate with alcohol content, as one might anticipate. Some odors do not have significant VOC sensor response (lime, vinegar), but do show appreciable pressure and temperature responses.

The experiment was repeated ten times for each analyte, and feature vectors containing the mean, derivative, and standard deviation were assembled from 0.5 second windows
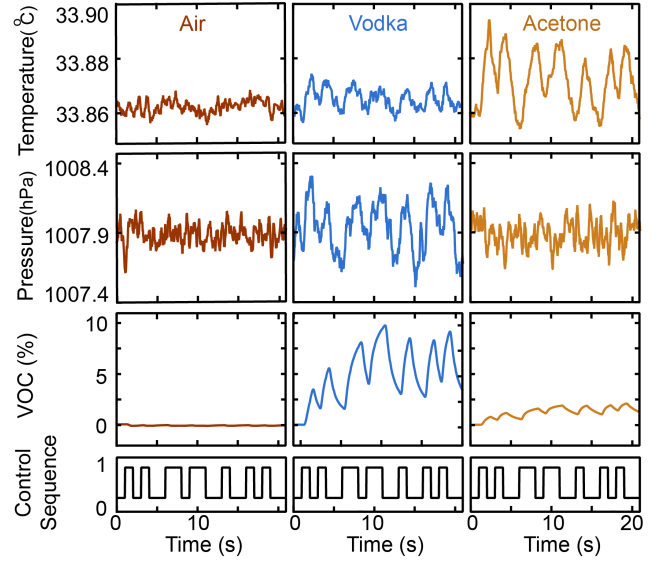

Fig. 4. Sensor time series for air, vodka, and acetone at a single location. In addition to the chemical sensor responsivity, both the direction and magnitude of the pressure and temperature changes carry information about the analyte.

of each of the 24 time series. We performed principal-component analysis (PCA) on the combined sensor data of the nine odor classes (Fig. 5b). Even with the first two principal components, tightly grouped clusters emerged. We then performed 2-fold cross-validation using a simple k-means algorithm over 1000 iterations. This classification approach is comparable to other e-nose demonstrations, and is one of many possible classification strategies (Table I).

A cross-validation accuracy of 90.9% was achieved using only the transient time series from the MOX sensors, compared to 79.8% if the data is condensed to only one average value per MOX sensor. Adding temperature and pressure data, accuracy improved to 95.8%. The confusion matrix in Fig. 5c and overlapping PCA clusters (Fig. 5b) show that most of the errors occurred between lime and vinegar, both of which are composites of the carboxyl group. Excluding data for lime and repeating the classification for the remaining odors yields an accuracy of 98.5%. These trends highlight the value of the complementary sensor time series, as well as the some of the challenges of comparing e-nose accuracies across different sets of odors.

IV. CONCLUSION

We have presented a new multi-parametric platform for odor classification, which is inspired by the fact that animals' olfactory systems are not purely chemical but also rely on mechanical and spatiotemporal cues. By incorporating transient sniffing features, air pressure, and temperature measurements, TruffleBot achieves high accuracy odor classification

TABLE I
SENSOR ARRAYS FOR ODOR CLASSIFICATION

|	Sensors	Measured Parameters	Array Size	Time Series	Analytes	Algorithm
This work	Metal oxide & Mechanical	chemical, pressure, temperature	8 (x3)	Yes	8	PCA
Wang et al, 2017 [22]	Metal oxide	chemical	12	No	5	PNN
Harun et al, 2009 [21]	Chemoresistive	chemical	900	No	4	PNN
Wojnowski et al, 2017 [10]	Electrochemical	chemical	7	No	8	SVM
Shulaker et al, 2017 [11]	Carbon nanotube FET	chemical	2048	No	7	PCA
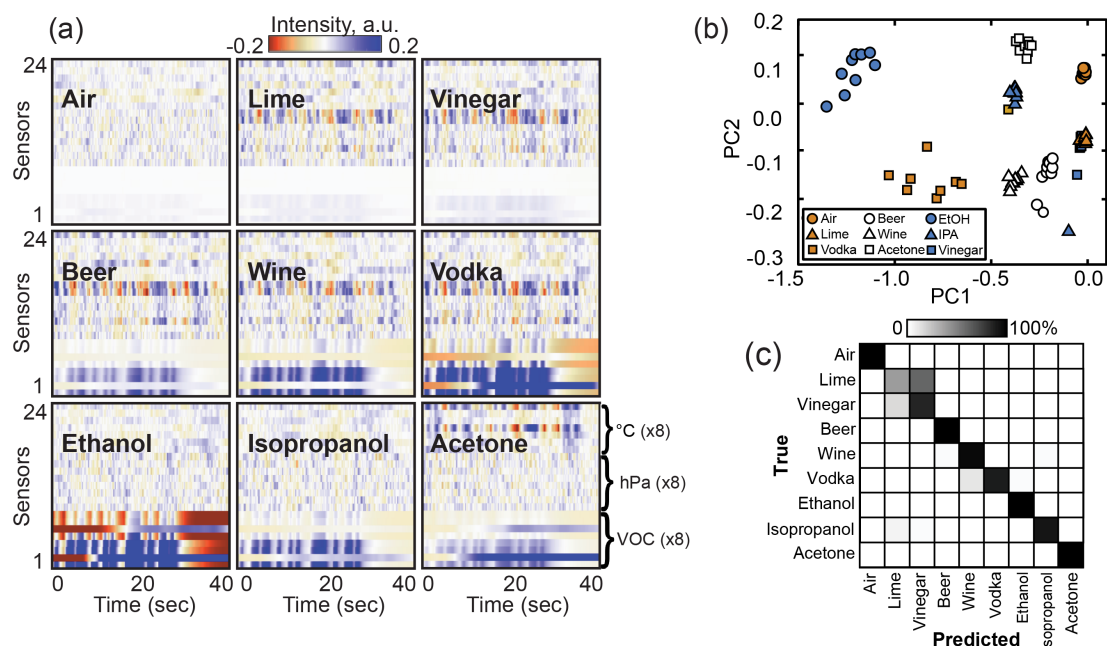
Fig. 5. (a) Data from all 24 sensors, in response to air and 8 analyte odors. (The mean value has been subtracted from each time series.) (b) A scatter plot of the first two principal components of the sensor data for the nine datasets. (c) Confusion matrix of the true odor vs. predicted odor. Most of the errors are conflating lime and vinegar, while the remaining odors are identified with high accuracy.

in a flexible and low cost platform. Similar arrangements will complement many types of chemical sensors. We note that these results were achieved without specific optimization of the fluid mechanical environment, and its success suggests that there will be many exciting opportunities in the near future for low-cost bio-inspired olfaction.

REFERENCES

[1] B. W. Ache and J. M. Young, "Olfaction: Diverse species, conserved principles," *Neuron*, vol. 48, no. 3, pp. 417 – 430, 2005.

[2] A. Diamond, M. Schmuker, A. Z. Berna, S. Trowell, and T. Nowotny, "Classifying continuous, real-time e-nose sensor data using a bio-inspired spiking network modelled on the insect olfactory system," *Bioinspiration and Biomimetics*, vol. 11, no. 2, p. 026002, 2016.

[3] K. Arshak, E. Moore, G. Lyons, J. Harris, and S. Clifford, "A review of gas sensors employed in electronic nose applications," *Sensor Review*, vol. 24, no. 2, pp. 181–198, 2004.

[4] P.-M. Lledo, G. Gheusi, and J.-D. Vincent, "Information processing in the mammalian olfactory system," *Physiological Reviews*, vol. 85, no. 1, pp. 281–317, 2005.

[5] M. Wachowiak, "All in a Sniff: Olfaction as a Model for Active Sensing," *Neuron*, vol. 71, no. 6, pp. 962–973, 2011.

[6] D. Mellon, "Smelling, feeling, tasting and touching: behavioral and neural integration of antennular chemosensory and mechanosensory inputs in the crayfish," *Journal of Experimental Biology*, vol. 215, no. 13, pp. 2163–2172, 2012.

[7] X. Grosmaitre, L. C. Santarelli, J. Tan, M. Luo, and M. Ma, "Dual functions of mammalian olfactory sensory neurons as odor detectors and mechanical sensors," *Nature Neuroscience*, vol. 10, pp. 348–354, 2007.

[8] A. D. Wilson and M. Baietto, "Applications and advances in electronic-nose technologies," *Sensors*, vol. 9, no. 7, pp. 5099–5148, 2009.

[9] G. Jasinski, P. Kalinowski, L. Wozniak, P. Koscinski, and P. Jasinski, "An electronic nose based on the semiconducting and electrochemical gas sensors," in *21st European Microelectronics and Packaging Conference (EMPC) Exhibition*, Sept 2017, pp. 1–4.

[10] W. Wojnowski, T. Majchrzak, T. Dymerski, J. Gbicki, and J. Namienik, "Portable electronic nose based on electrochemical sensors for food quality assessment," *Sensors*, vol. 17, no. 12, 2017.

[11] M. M. Shulaker, G. Hills, R. Park, R. T. Howe, K. Sawaswat, H. S. P. Wong, and S. Mitra, "Three-dimensional integration of nanotechnologies for computing and data storage on a single chip," *Nature*, vol. 547, pp. 74–78, Jul 2017.

[12] R. Huerta, T. Mosqueiro, J. Fonollosa, N. F. Rulkov, and I. Rodriguez-Lujan, "Online decorrelation of humidity and temperature in chemical sensors for continuous monitoring," *Chemometrics and Intelligent Laboratory Systems*, vol. 157, pp. 169 – 176, 2016.

[13] Y. Chen, G. Fu, Y. Zilberman, W. Ruan, S. K. Ameri, E. Miller, and S. Sonkusale, "Disposable colorimetric geometric barcode sensor for food quality monitoring," in *2017 19th International Conference on Solid-State Sensors, Actuators and Microsystems (TRANSDUCERS)*, 2017, pp. 1422–1424.

[14] L. Mølhave, B. Bach, and O. Pedersen, "Human reactions to low concentrations of volatile organic compounds," *Environment International*, vol. 12, no. 1, pp. 167 – 175, 1986.

[15] C. Fan, G.-S. Wang, Y.-C. Chen, and C.-H. Ko, "Risk assessment of exposure to volatile organic compounds in groundwater in taiwan," *Science of The Total Environment*, vol. 407, no. 7, pp. 2165 – 2174, 2009.

[16] H. Li, C. S. Boling, and A. J. Mason, "Cmos amperometric adc with high sensitivity, dynamic range and power efficiency for air quality monitoring," *IEEE Transactions on Biomedical Circuits and Systems*, vol. 10, no. 4, pp. 817–827, Aug 2016.

[17] K. T. Tang, S. W. Chiu, M. F. Chang, C. C. Hsieh, and J. M. Shyu, "A low-power electronic nose signal-processing chip for a portable artificial olfaction system," *IEEE Transactions on Biomedical Circuits and Systems*, vol. 5, no. 4, pp. 380–390, Aug 2011.

[18] S. W. Chiu, J. H. Wang, G. T. Lin, C. L. Chang, H. Chen, and K. T. Tang, "Towards a fully integrated electronic nose soc," in *2012 IEEE 55th International Midwest Symposium on Circuits and Systems (MWSCAS)*, 2012, pp. 166–169.

[19] P. Shakya, E. Kennedy, C. Rose, and J. K. Rosenstein, "Correlated transmission and detection of concentration-modulated chemical vapor plumes," *IEEE Sensors Journal*, vol. 18, no. 16, pp. 6504–6509, Aug 2018.

[20] E. Kennedy, P. Shakya, M. Ozmen, C. Rose, and J. K. Rosenstein, "Spatiotemporal information preservation in turbulent vapor plumes," *Applied Physics Letters*, vol. 112, no. 26, p. 264103, 2018.

[21] F. C. Harun, J. Taylor, J. Covington, and J. Gardner, "An electronic nose employing dual-channel odour separation columns with large chemosensor arrays for advanced odour discrimination," *Sensors and Actuators B: Chemical*, vol. 141, no. 1, pp. 134 – 140, 2009.

[22] Y. Wang, J. Xing, and S. Qian, "Selectivity enhancement in electronic nose based on an optimized dqn," *Sensors*, vol. 17, no. 10, 2017.